Pergamon

Bioorganic & Medicinal Chemistry, Vol. 3, No. 6, pp. 631–646, 1995

0968-0896/95 $9.50 + .00

0968-0896(95)00051-8

NMR Structure of d(CGCA$_3$T$_3$GCG)$_2$:Tren-Microgonotropen-b:Zn(II) Complex and Solution Studies of Metal Ion Complexes of Tren-Microgonotropen-b Interacting with DNA

Andrei Blaskó, Kenneth A. Browne, and Thomas C. Bruice*

Department of Chemistry, University of California, Santa Barbara, CA 93106, U.S.A.

Abstract—The solution structure of a 1:1 complex of zinc tren-microgonotropen-b {**6b**:Zn(II)} with d(CGCAAATTTGCG)$_2$ has been determined by 2D nuclear Overhauser effect ^{1}H NMR spectroscopy and restrained molecular modeling. The exchangeable and nonexchangeable proton resonances of d(CGCA$_3$T$_3$GCG)$_2$:**6b**:Zn(II) indicate that the Zn(II) is interacting in the A+T-rich region of the dsDNA and the tren region of **6b**, while ^{31}P NMR shows interaction of the Zn(II) with the phosphate backbone. Proton chemical shift differences between d(CGCA$_3$T$_3$GCG)$_2$:**6b**:Zn(II) and d(CGCA$_3$T$_3$GCG)$_2$:**6b** are in agreement with the polyamino substituent of **6b** {-(CH$_2$)$_4$N(CH$_2$CH$_2$)N-(H$_2$CH$_2$NH$_2$)$_2$} forming a four-coordinated Zn(II) complex similar to that found in the X-ray structure of 'tren-chloride':Zn(II). The P$_9$ and P$_{10}$ phosphate oxygens that are held by hydrogen bonding to the tren substituent of **6b** in the DNA:**6b** complex become ligands to the tren-complexed Zn(II) in DNA:**6b**:Zn(II). To do so there is a 2 Å decrease in the adjacent phosphate-to-phosphate distance at the Zn(II) binding site. This motion brings about an increased bend of 14.6° in the helical axis of d(CGCA$_3$T$_3$GCG)$_2$:**6b**:Zn(II) compared to that found in d(CGCA$_3$T$_3$GCG)$_2$:**6b**. Single stranded cleavage of linear DNA fragments was not observed in the presence of **6b** and Fe(II), Co(II), Ni(II), Cu(II), Zn(II), La(III) or Ce(III); this is likely due to the metal ion being sequestered as in the structure of d(CGCA$_3$T$_3$GCG)$_2$:**6b**:Zn(II) complex. Supercoiled DNA was susceptible to cleavage by **6b**:Cu(II) in the presence of O$_2$ and a reducing agent.

Introduction

The interactions of metal ions with nucleotides are essential in basic metabolic processes.[1] In order to understand the interactions of the metal ions with ligand–dsDNA complexes, knowledge of the stereochemistry around the metal ion when ligated to the dsDNA complexes and the conformational changes of the dsDNA and ligands which occur upon the metal ion binding is necessary. Currently, about 100 DNA oligonucleotide structures have been determined (by NMR or X-ray crystallography), many of which are dodecamers that adopt the B-DNA form. Many drug–DNA complexes involve only the minor groove with stoichiometries of 1:1 (berenyl, pentamidine[2]), 2:1 (distamycin, Hoechst,[3–5] the heterocomplex of distamycin and 2-imidazole-distamycin[6]), or 4:1 (distamycin[3]). There is evidence that metal ions can induce minor groove {Mg(II)(chromomycin)$_2$}[7] or major groove {Δ- and Λ-[Ru(1,10-phenanthroline)]$^{2+}$}[8] ligand bindings. However, little work has been done in the area regarding the interactions of metal ions with the phosphate backbone by NMR spectroscopy. The first example of formation of a drug–DNA complex which appears to be centered on the phosphate backbone is a metallocene {cyclopentadienyl–Mo complex, Cp$_2$Mo-(H$_2$O)(H$_3$O)$^+$} which can lose one or both ancillary ligands to become covalently attached to the dsDNA backbone via either one or two phosphate(O) bonds.[9]

Microgonotropens are tripyrrole peptide derivatives which bind to A+T-rich regions of the minor groove of dsDNA and extend to the major groove via a polyamine substituent designed to reach the phosphate backbone of the DNA.[10–14] The dien-microgonotropens (**5abc**) and tren-microgonotropens (**6ab**) are compared in Chart 1. In this study, the three-dimensional (3D) solution structure of the 1:1:1 complex of **6b** with d(CGCA$_3$T$_3$GCG)$_2$ and Zn(II) has been determined by use of nuclear Overhauser effect spectroscopy (NOESY) and restrained molecular modeling (RM). Also, the conformational changes which occur in the dsDNA and **6b** upon Zn(II) ligation are shown. Additional evidence for such conformational changes is demonstrated by gel electrophoretic mobility shift assays. In a search for hydrolytic cleavage of pBR322 supercoiled DNA by **6b**:metal ion complexes with the DNA, the following metal ions were studied: Co(II), Zn(II), Ni(II), La(III) and Ce(III). The NOESY/RM refined structure of d(CGCA$_3$T$_3$GCG)$_2$:**6b**:Zn(II) helps explain the inefficiency of metal ion catalysis of DNA hydrolysis.

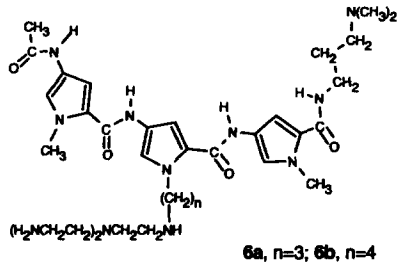

6a, n=3; 6b, n=4

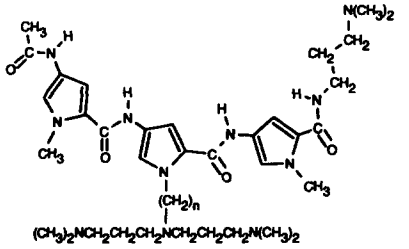

5a, n=3; 5b, n=4; 5c, n=5

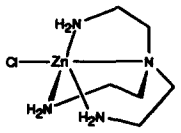

AEZNPB

Results

Equilibrium association constants of 6b with the hexadecamer d(GGCGCAAATTTGGCGG)/d(CCGCCA-AATTTGCGCC) in the presence of Zn(II)

Equilibrium association constants were assessed in aqueous solutions at 35 °C (2.8 mL solutions containing 0.01 M phosphate buffer, pH 7.0, and 0.01 M KCl). Equilibrium constants were determined by the competition of the dye Hoechst 33258 (Ht) with **6b**:Zn(II) for the A_3T_3 minor groove binding site (an extension of Ht alone binding to dsDNA). As shown previously,[12] monitoring the increase in fluorescence intensity as the association of **Ht** with the hexadecamer displaces prebound nonfluorescent ligands is an excellent method for determining equilibrium binding constants. Scheme 1 shows the equilibria for complexation of one and two Ht species to the

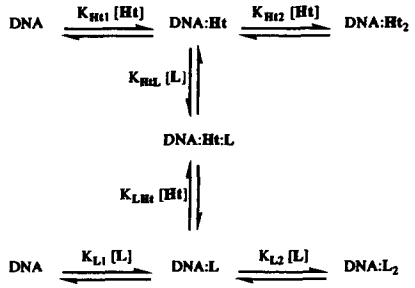

Scheme 1.

hexadecamer with zero, one and two ligands, L, [where L = **6b** or **6b**:Zn(II)] binding to the hexadecamer and also the simultaneous binding of one Ht and one L at the same site. Equation 1, derived from Scheme 1, relates each of the equilibrium binding constants, the

$$F = \frac{\Sigma\Phi\ K_{Ht1}[Ht]\ (0.5+K_{Ht2}\ [Ht]\ +0.5\ K_{HtL}\ [L]\ Q')}{1+K_{Ht1}[Ht]+K_{Ht1}K_{Ht2}[Ht]^2+K_{Ht1}K_{HtL}[Ht][L]+K_{L1}[L]+K_{L1}K_{L2}[L]^2} \quad (1)$$

total fluorescence ($\Sigma\Phi$), and [L] in terms of fluorescence (F) and [Ht]. The rationale behind Scheme 1 and the subsequent derivation of Eq. 1 have been described in considerable detail.[12] The values of K_{Ht1} = 2.01×10^7 M^{-1} and K_{Ht2} = 1.67×10^9 M^{-1} used in this study [determined in the presence of 1.0×10^{-7} M Zn(II)] are comparable to those values determined in the absence of Zn(II) (K_{Ht1} = 4.0×10^7 M^{-1} and K_{Ht2} = 1.2×10^9 M^{-1}).[14] The concentration independent static quenching term (Q'), included in Eq. 1 to account for the lessened fluorescent emission of the DNA:Ht:L complex compared to the DNA:Ht and DNA:Ht_2 complexes, is very nearly the same for **6b** ± Zn(II) (Table 1). The equilibrium association constants calculated as best fits to the experimental data points for **6b**:Zn(II) with Eq. 1 are compared with the same values for **6b** alone in Table 1. Plots of fluorescence (F) vs [**Ht**] using these constants at 8.0×10^{-9}, 1.0×10^{-8}, and 1.2×10^{-8} M ligand and 5.0×10^{-9} M in hexadecameric duplex are shown in Figure 1.

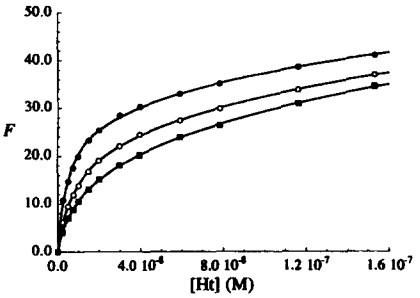

Figure 1. Plot of fluorescence (F, in arbitrary units) vs Hoechst 33258 (**Ht**) concentration at pH 7.0 and 35 °C for **6b** at 8.0×10^{-9} M (—l—), 1.0×10^{-8} M (—m—), and 1.2×10^{-8} M (—n—) in the presence of 5.0×10^{-9} M hexadecamer d(GGCGCA$_3$T$_3$GGCGG)/d(CCGCCA$_3$T$_3$GCGCC) and 1.0×10^{-7} M $ZnCl_2$. The theoretical curves which fit the points were computer generated by use of Eq 1.

Table 1. Equilibrium constants for the association of **6b** ± Zn(II) to d(GGCGCAAATTTGGCGG)/d(CCGCCAAATTTGCGCC) at 35 °C

Constants	**6b**[a]	**6b**:Zn(II)[b]
K_{L1}	7.58×10^8 M^{-1}	4.67×10^8 M^{-1}
K_{L2}	9.46×10^8 M^{-1}	1.02×10^9 M^{-1}
$K_{L1}K_{L2}$	7.17×10^{17} M^{-2}	4.76×10^{17} M^{-2}
K_{Ht}	2.23×10^{10} M^{-1}	4.09×10^{10} M^{-1}
K_{LHt}	1.18×10^9 M^{-1}	1.75×10^9 M^{-1}
Q'	0.64	0.69

[a]Values determined previously.[14] [b]The mean values of the constants are from duplicate titration experiments performed at 8.0×10^{-9}, 1.0×10^{-8}, and 1.2×10^{-8} M **6b** in the presence of 1.0×10^{-7} M $ZnCl_2$.

Titration of d(CGCA$_3$T$_3$GCG)$_2$:6b complex with $ZnCl_2$

The titration was followed by ^{1}H NMR and performed in 0.25 mol equiv. steps in 9:1 H_2O:D_2O at 21 °C and at a concentration of 2.5×10^{-3} M in d(CGCA$_3$T$_3$GCG)$_2$:**6b** complex. The G≡C and A=T imino protons of the

d(CGCA$_3$T$_3$GCG)$_2$:**6b** complex resonate at 12.5 – 13.2 and 13.4 – 14.1 ppm, respectively (Fig. 2). On titrating the d(CGCA$_3$T$_3$GCG)$_2$:**6b** complex with $ZnCl_2$, only the A=T resonance at 13.50 ppm changes while observing up to 1:1 mol equiv. of Zn(II):dsDNA:**6b** complex. The resonance at 13.50 ppm decreases and becomes a shoulder on the appearing resonance at 13.47 ppm at 0.5 and 0.75 mol equiv. of Zn(II):dsDNA:**6b**. At 1:1 mol equiv. of Zn(II):dsDNA:**6b**, there is only a single resonance in the 13.4 – 13.6 ppm range; this does not change further when titrating up to 1.2:1 Zn(II)/dsDNA:**6b**. No significant changes occur at the other imino protons. Also, there are no significant changes in the amino proton resonances when monitoring the titration spectra in the 8.3 – 9.7 ppm region (data not shown). When observing the 1.0 – 3.5 ppm region, we saw changes between 2.6 and 2.8 ppm but no changes at the T-CH_3 proton resonances (1.1 – 1.7 ppm) (Fig. S1). We saw a 0.1 ppm upfield shift of the ^{31}P resonances when recording the ^{31}P spectra before and after addition of one mol equiv. of Zn(II) per dsDNA:**6b** complex (2.5×10^{-3} M). There were no significant changes of the ^{31}P NMR line shape except for the resonances centered at –1.9 ppm which broaden significantly (40–100 Hz) upon Zn(II) addition with a corresponding loss in intensity (Fig. S2).

*The assignment of the resonances of **6b***

The assignment of the resonances of **6b** in D_2O in the d(CGCA$_3$T$_3$GCG)$_2$:**6b** complex has been reported.[15] These assignments were used as leads for the assignment of the resonances of **6b** in the dsDNA:**6b**:Zn(II) complex. The **6b** chemical shifts in the d(CGCA$_3$T$_3$GCG)$_2$:**6b**:Zn(II) complex are summarized in Table S1. The H2, H4 and H6 pyrrole resonances of **6b** (see Scheme 2a for notations) are found in the 6.5 – 6.8 ppm region (Fig. S3). H4 and H6 give NOEs with the aromatic adenosine A_{-8}H2 proton of the (–) strand while the H2 proton gives an intramolecular **6b** interaction with H4. We did not see any NOE interactions between H4 and H6 as was seen in the complex without Zn(II). The H1, H3 and H5 resonances of **6b** were assigned using their intramolecular interactions with the CH_2^n(i) methylenes of the central hydrocarbon linker and with the CH_3^{R1} group of the acetamide substituent (Fig. 3). The assignment of the **6b** resonances was confirmed by the NOE enhancements in the NOESY spectrum (Figs S4 and S5).

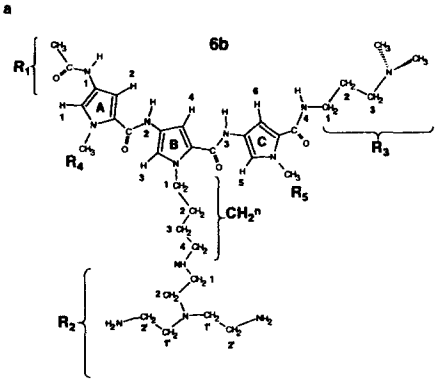

Scheme 2.

*Assignment of ^1H chemical shifts of d(CGCA$_3$T$_3$GCG)$_2$ in the d(CGCA$_3$T$_3$GCG)$_2$:**6b**:Zn(II) complex*

Upon Zn(II) complexation, the existence of two sets of Watson–Crick G≡C and A=T resonances and two sets of thymidine CH_3 resonances (Figs 2 and S5) at 1:1 mol equiv. of Zn(II)/d(CGCA$_3$T$_3$GCG)$_2$:**6b** is indicative of the unchanged asymmetric and monomeric binding of **6b** to the DNA molecule. The aromatic base protons H8 and H6 of the purines and pyrimidines were assigned through their interactions with the (n-1)H2"

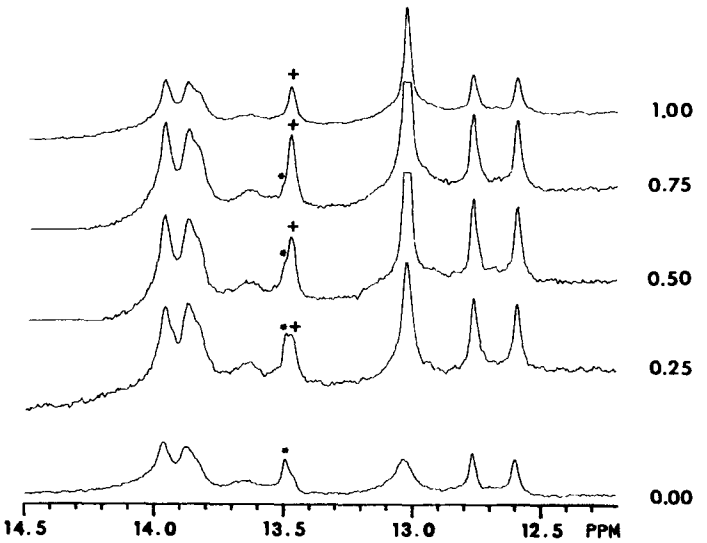

Figure 2. ^1H NMR titration of 2.5×10^{-3} M d(CGCA$_3$T$_3$GCG)$_2$:**6b** in 9:1 H_2O/D_2O (10 mM phosphate buffer, pH 7.0, 10 mM KCl) with $ZnCl_2$ at the indicated mole ratios of Zn(II)/d(CGCA$_3$T$_3$GCG)$_2$:**6b**. The titration was followed by the disappearance of the resonance marked with asterisks and the appearance of the resonance marked with (+) signs.

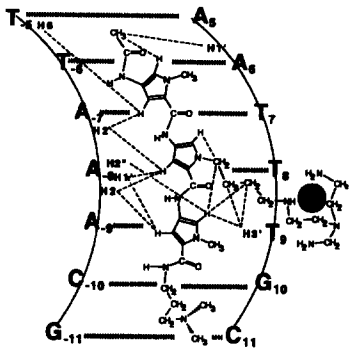

Figure 3. Schematic representation of the dsDNA–**6b** intracomplex and **6b** intramolecular NOE interactions (represented by broken lines) in the d(CGCA$_3$T$_3$GCG)$_2$:**6b**:Zn(II) complex. The sugar protons are labeled with prime and double prime (see Experimental section) and placed next to the residue to which they belong. The aromatic A$_{-7}$A$_{-8}$ H2 protons give NOE interactions with the aromatic pyrrole protons of **6b**, defining the position of the tripyrrole peptide moiety in the A+T-rich region.

sugar protons and their own H1' protons. The thymidine CH_3 protons were assigned through the interactions with their own base protons (H6) and through their interactions with the neighboring thymidine CH_3s or A_6H8 and A_{-7}H8 protons for the (+) and (–) strands, respectively (Fig. 4, Scheme 2b, and Table 2). The assignment of the dsDNA resonances in the d(CGCA$_3$T$_3$GCG)$_2$:**6b** complex[15] was used as leads in the assignment of the resonances in the d(CGCA$_3$T$_3$GCG)$_2$:**6b**:Zn(II) complex. The sugar proton resonances were assigned from the NOESY spectrum of the Zn(II) complex (Figs 4, S4–S7). Expansion of the NOESY spectrum in the (1.1–3.0) × (6.8–8.4) ppm region shows the general pattern of NOESY interactions of H6/8–H2'2", H6/8–T$_i$CH$_3$, and T$_i$CH$_3$–T$_{i+1}$CH$_3$ (Fig. 4 and Table 3) used for the assignment of sugar H2'2" proton resonances (Table 2). The signals of $T_7T_{-6}CH_3$ were used as starting signals for the sequential assignment of the dsDNA resonances (Fig. 4 and Table 3) as in previous investigations of d(CGCA$_3$T$_3$GCG)$_2$, d(CGCA$_3$T$_3$GCG)$_2$:**5c** and d(CGCA$_3$T$_3$GCG)$_2$:**6b** structures.[11,15] The $T_7T_{-6}CH_3$ signals were used for the assignment of A_6A_{-7}H8, $T_7T_8T_9$H6 and $T_{-4}T_{-5}T_{-6}$H6 proton resonances (Fig. 4). As before, the convention used is that the (+) strand is defined as the DNA strand upon which the ligand reaches up to and complexes the phosphodiester backbone while the (–) strand is the complementary DNA strand. From the known resonances of cytidine H6/5 we assigned the remaining

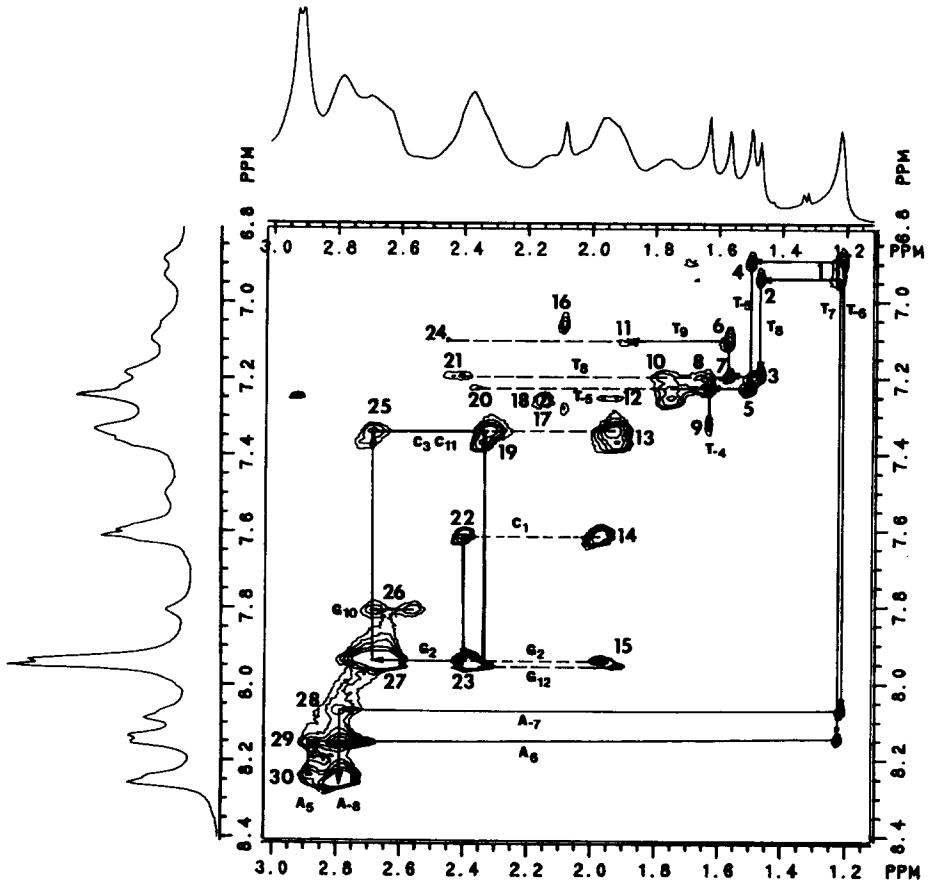

Figure 4. Expansion of the NOESY spectrum in the (1.1 – 3.0) × (6.8 – 8.4) ppm region of d(CGCA$_3$T$_3$GCG)$_2$:**6b**:Zn(II), 2.5 × 10^{-3} M in 99.96% D_2O containing 10 mM KCl and 10 mM phosphate buffer, pH 7.0 at 10 °C (τ_m = 180 ms). **1.** T_7H6–T_7CH_3, T_{-6}H6–$T_{-6}CH_3$; **2.** T_7H6–T_8CH_3; **3.** T_8H6–T_8CH_3; **4.** T_{-6}H6–$T_{-5}CH_3$; **5.** T_{-5}H6–$T_{-5}CH_3$; **6.** T_9H6–T_9CH_3; **7.** T_8H6–T_9CH_3; **8.** T_{-5}H6–T_{-4} CH_3; **9.** T_{-4}H6–$T_{-4}CH_3$; **10.** H5–CH_2"(2); **11.** T_9H6–T_9H2'; **12.** H5–T_8H2'; **13.** C_3C_{11}H6–C_3C_{11}H2'; **14.** C_1C_{-12}H6–C_1C_{-12}H2'; **15.** G_2G_{12}H8–C_1C_{11}H2'; **16.** H1–CH_3^{R1}; **17.** H3–CH_3^{R1}; **18.** H5–CH_2"(3); **19.** C_3C_{11}H6–C_3C_{11}H2"; **20.** T_{-5}H6–T_{-5}H2"; **21.** T_8H6–T_7H2"; **22.** C_1C_{-12}H6–C_1C_{-12}H2"; **23.** G_2G_{12}H8–C_1C_{11}H2"; **24.** T_9H6–$T_9$2"; **25.** C_3C_{11}H6–G_2G_{10}H2" **26.** G_{10}H8–G_{10}2'2"; **27.** G_2G_{12}H8–G_2G_{12}H2", G_2H8–G_2H2'; **28.** A_{-7}H8–A_{-7}H2"; **29.** A_6H8–A_5H2'2", A_{-9}H8–A_{-9}H2'2"; **30.** A_4A_5H8–A_4A_5H2'2", A_{-8}H8–A_{-8}H2'2"; **31.** H5–A_8H2".

Table 2. ^{1}H Chemical shifts for d(CGCA$_3$T$_3$GCG)$_2$ in the 1:1 complex of d(CGCA$_3$T$_3$GCG)$_2$:**6b** with Zn(II) in D$_2$O[a]

Base	H1'	H2'	H2"	H3'	H4'	H5'	H5"	H6/8	H2/5/CH$_3$
(+) Strand									
$^{5'}C_1$	5.72	1.98	2.40	4.71	4.06	4.07	3.73	7.62	5.88
G_2	5.85	2.65	2.72	4.96	4.33	4.40	4.37	7.94	
C_3	5.75	1.92	2.35	4.84	4.18	4.19	4.11	7.38	5.45
A_4	5.84	2.77	2.87	5.06	4.38	4.49	4.22	8.22	7.20
A_5	5.56	2.77	2.83	5.07	nd[b]	4.46	4.38	8.27	6.96
A_6	5.87	2.71	2.75	5.07	4.22	4.40	4.22	8.16	7.50
T_7	5.37	1.93	2.43	4.63	nd	4.02	3.89	6.94	1.22
T_8	5.56	1.98	2.40	4.63	3.70	3.90	3.37	7.19	1.46
T_9	5.55	1.89	2.45	4.80	nd	4.23	4.17	7.11	1.56
G_{10}	5.81	2.56	2.64	4.98	4.03	4.40	4.15	7.82	
C_{11}	5.70	1.93	2.34	4.82	4.05	4.18	4.15	7.36	5.43
G_{12}	6.16	2.39	2.65	4.69	4.20	4.18	4.07	7.96	
(–) Strand									
$^{5'}C_{-12}$	5.72	1.98	2.40	4.69	4.06	3.98	3.73	7.62	5.88
G_{-11}	5.85	2.65	2.72	4.92	4.33	4.40	4.37	7.94	
C_{-10}	5.75	1.92	2.35	4.84	4.18	4.19	4.11	7.38	5.45
A_{-9}	5.89	2.77	2.87	5.06	nd	4.49	4.22	8.15	7.53
A_{-8}	5.55	2.88	2.93	5.07	nd	4.46	4.38	8.25	8.10
A_{-7}	5.87	2.74	2.80	5.07	nd	4.40	4.22	8.07	8.12
T_{-6}	5.70	1.93	2.34	4.64	nd	4.15	3.90	6.89	1.21
T_{-5}	6.18	1.98	2.37	4.63	3.70	4.00	3.85	7.23	1.49
T_{-4}	5.75	1.98	2.42	4.64	nd	4.15	4.17	7.33	1.63
G_{-3}	5.81	2.56	2.64	5.00	4.01	4.10	3.98	7.92	
C_{-2}	5.70	1.93	2.34	4.84	4.05	4.18	4.15	7.36	5.43
G_{-1}	6.16	2.39	2.65	4.69	4.20	4.18	4.07	7.96	

[a]δ in ppm relative to DSS at 10 °C; [dsDNA] = 2.5 × 10^{-3} M (10 mM phosphate buffer pH 7.0, 10 mM KCl). The Watson–Crick imino protons (recorded in 9:1 H$_2$O:D$_2$O) are in the range: A=T 13.4 – 14.1 and G≡C 12.5 – 13.2 ppm.
[b]Not determined.

Table 3. Comparison of the sequential NOEs for: (a) the 1:1 complex of d(CGCA$_3$T$_3$GCG)$_2$ with **6b** and (b) for the 1:1 complex of Zn(II) with d(CGCA$_3$T$_3$GCG)$_2$:**6b**.

(a) (+) Strand:	C_1	G_2	C_3	A_4	A_5	A_6	T_7	T_8	T_9	G_{10}	C_{11}	G_{12}
H6/8–CH$_3$/H5/6/8					o	o	o	o			o	o
H6/8/5–H1'	o	o								o	o	
H6/8/CH$_3$–H2"	o	o	o		o	o	o	o		o	o	o
H6/8–H3'											o	o
H2/CH$_3$–H2/CH$_3$				o	o		o	o				
(a) (–) Strand:	C_{-12}	G_{-11}	C_{-10}	A_{-9}	A_{-8}	A_{-7}	T_{-6}	T_{-5}	T_{-4}	G_{-3}	C_{-2}	G_{-1}
H6/8–CH$_3$/H5/6/8				o	o	o	o	o	o		o	o
H6/8–H1'				o	o				o	o		
H6/8/CH$_3$–H2"		o	o		o	o	o	o			o	o
H6/8–H3'											o	o
H2/CH$_3$–H2/CH$_3$				o	o	o	o	o	o			
(b) (+) Strand:	C_1	G_2	C_3	A_4	A_5	A_6	T_7	T_8	T_9	G_{10}	C_{11}	G_{12}
H6/8–H$_3$/H5/6/8							o	o			o	o
H6/8/5–H1'	o	o	o									
H6/8/CH$_3$–H2'2"	o	o	o		o	o	o	o		o	o	o
H6/8–H3'											o	o
H2/CH$_3$–H2/CH$_3$							o	o				
H2–H5"						o	o					
H5–H2"		o	o							o	o	
(b) (–) Strand:	C_{-12}	G_{-11}	C_{-10}	A_{-9}	A_{-8}	A_{-7}	T_{-6}	T_{-5}	T_{-4}	G_{-3}	C_{-2}	G_{-1}
H6/8–CH$_3$/H5/6/8							o	o	o		o	o
H6/8/5–H1'	o	o	o									
H6/8/CH$_3$–H2'2"	o	o	o							o	o	o
H6/8–H3'											o	o
H2/CH$_3$–H2/CH$_3$							o	o				
H5–H2"		o	o							o	o	

aromatic resonances. In the assignment process we also used the fact that **6b** binds into the minor groove at A+T-rich regions.[14] The guanosine H8 resonances (7.8 – 8.0 ppm) were used to define the $C_1G_2G_{12}$H1' and T_{-4}H1' resonances (Fig. S3). No NOE interactions were seen between G_{10}H8 and any of the H3' or H5'5" protons nor between adenosine H8 and H5'5" protons. The H4' and H5'5" proton resonances were resolved (where possible) using their NOEs with H1' protons (Fig. S6 and Table 2). A survey of the sequential NOEs for the DNA selected protons in the ligated dsDNA is shown in Table 3.

Interactions between d(CGCA$_3$T$_3$GCG)$_2$ and 6b:Zn(II)

The position of tren-microgonotropen-b (**6b**) in the A+T-rich region of the minor groove of d(CGCA$_3$T$_3$GCG)$_2$ does not significantly change upon Zn(II) complexation as evidenced by the imino protons' region (Fig. 2). Most of the same NOE interactions found in the d(CGCA$_3$T$_3$GCG)$_2$:**6b** complex were also found in the Zn(II) complex. However, some of them were not observed and, hence, fewer NOEs were seen (Table 3). We saw one NOE interaction in the Zn(II) complex (between A_6H8 and T_7H2") which was not seen in the dsDNA:**6b** complex. Expansion of the NOESY spectrum in the (5.3 – 8.5) × (5.2 – 8.5) ppm region shows strong NOE interactions between the tripyrrole peptide H2, H4 and H6 protons of **6b** and the minor groove aromatic protons A_{-8}H2 and A_{-7}H2 as well as weaker NOEs for H4 and H6 with the sugar A_{-8}H1' proton (Figs S3 and S6). The acetamido CH_3^{R1} methyl protons of **6b** give NOE with A_6H1' (Fig. S4) defining the orientation of the **6b** molecule in the minor groove. The tren substituent of **6b** {-$(CH_2)_4$N(CH_2CH_2)N-$(CH_2CH_2NH_2)_2$} strongly interacts with the sugar protons of T_9. We saw NOEs between T_9H3' and the hydrocarbon linker protons CH_2^n(2) and CH_2^n(3) (Fig. S4). An intracomplex interaction between T_9H3' and H5 was also observed (Fig. S7). We did not see any NOEs between the R3 propylamino substituent of **6b** and d(CGCA$_3$T$_3$GCG)$_2$ and we saw only one weak NOE between CH_3^{R3} and CH_2^{R3}(1). The intracomplex and **6b** intraresidual NOE interactions are shown in Figure 4.

As a result of the Zn(II) complexation, induced chemical shift differences ($\Delta\delta$) were observed in certain proton resonances (Fig. 5). For the H1', H2' and H2" proton resonances, the chemical shift differences are 0.1 – 0.2 ppm, for H5' and H5" they are *ca* 0.1 ppm, and for H3' and H6/8 they are < 0.05 ppm. The $\Delta\delta$ extends beyond the binding site of dsDNA due to distortion of the dsDNA upon Zn(II) complexation by the tren moiety of **6b**. The chemical shift differences are greater for the H1' protons (minor groove pointers) than for any other selected protons. The increase in $\Delta\delta$ follows the order H6/8 < H3' < H5'5" < H2' < H2" < H1'. The $\Delta\delta$ for the tren substituent of **6b** has values of 0.05 ppm for CH_2^n(4) and CH_2^{R2}(2') and 0.1 ppm for CH_2^{R2}(1') (Fig. 5 and Table S1). All of the CH_3 protons give downfield shifts (0.02 – 0.03 ppm) as did the H2 and H3 protons of the central pyrrole. No chemical shift differences were seen for the other pyrrole protons.

Distance calculations and restrained molecular modeling refinements

For the d(CGCA$_3$T$_3$GCG)$_2$:**6b**:Zn(II) complex, we found 156 intramolecular dsDNA interactions for both NMR-nonequivalent strands. In refining the DNA distances of the d(CGCA$_3$T$_3$GCG)$_2$:**6b**:Zn(II) complex, 30 distance constraints were used (Table 4 and Fig. 4). These intramolecular interactions represent the only well separated cross peaks (Table 4). Essentially the same minimization procedure used previously[11,15] was employed to obtain the most probable solution structure of the d(CGCA$_3$T$_3$GCG)$_2$:**6b**:Zn(II) complex (Fig. 6). Only three of the refined distances were greater than ± 0.4 Å from the NOE calculated distances (Table 4). The ROESY spectrum (Fig. S8) confirmed most of the NOESY enhancements.

The dsDNA bending angle in d(CGCA$_3$T$_3$GCG)$_2$:**6b** is increased by 14.6° (from 21.0 to 35.6°) on formation of d(CGCA$_3$T$_3$GCG)$_2$:**6b**:Zn(II) (Fig. S9). The width of the minor groove widens by 1.3 Å in the $G_{10}A_{-7}$ region from 11.9 to 13.2 Å upon Zn(II) ligation and there were only slight changes in the positioning of **6b** inside the minor groove. The ligand (**6b**) binds 4.4 – 7.9 and 6.2 – 6.8 Å from the (–) and (+) strands, respectively, when examining the regions from T_{-5} to A_{-7} and G_{10} to T_8. In addition, the Zn(II) complexation to d(CGCA$_3$T$_3$GCG)$_2$:**6b** lengthens dsDNA by 2.3 Å compared to the solution structure of the dodecamer alone[11] as is evidenced by the unit height (35.5 Å/repeat). Compared to B-DNA,[16] this is due to a combination of a relatively wound helix (turn angle = 35.5°/bp), a large axial rise (3.50 Å/bp), and a large B-DNA helical rise (10.1 bp/repeat). The two phosphate groups that are on either side of the tren:Zn(II) moiety (P_9 and P_{10}) are only 4.6 Å apart while the remaining adjacent phosphates in d(CGCA$_3$T$_3$GCG)$_2$:**6b**:Zn(II) and in four crystal structures containing the d(CGCA$_3$T$_3$GCG)$_2$ sequence have mean distances of 6.6 ± 0.6 and 6.7 ± 0.3 Å, respectively. In the solution structure, the molecular contact surface area between d(CGCA$_3$T$_3$GCG)$_2$ and **6b**[15] is 532 Å^2 while in the **6b**:Zn(II) complex it is 471 Å^2.

In order to ensure that the dramatic changes found in the bending angle were due to the experimental NOEs and not to the CHARMm force field and large electrostatic potential between the Zn(II) and two adjacent PO_4^- moieties, several tests of the constraints and charge were performed. In the first test minimization, all parameters were kept exactly the same as for the solution structure of d(CGCA$_3$T$_3$GCG)$_2$:**6b**:Zn(II) except that NOE constraints were not included. This new structure's bend angle was only 15.8° even though the adjacent phosphates were now 4.0 Å apart. The second and third test minimizations were also performed without NOE

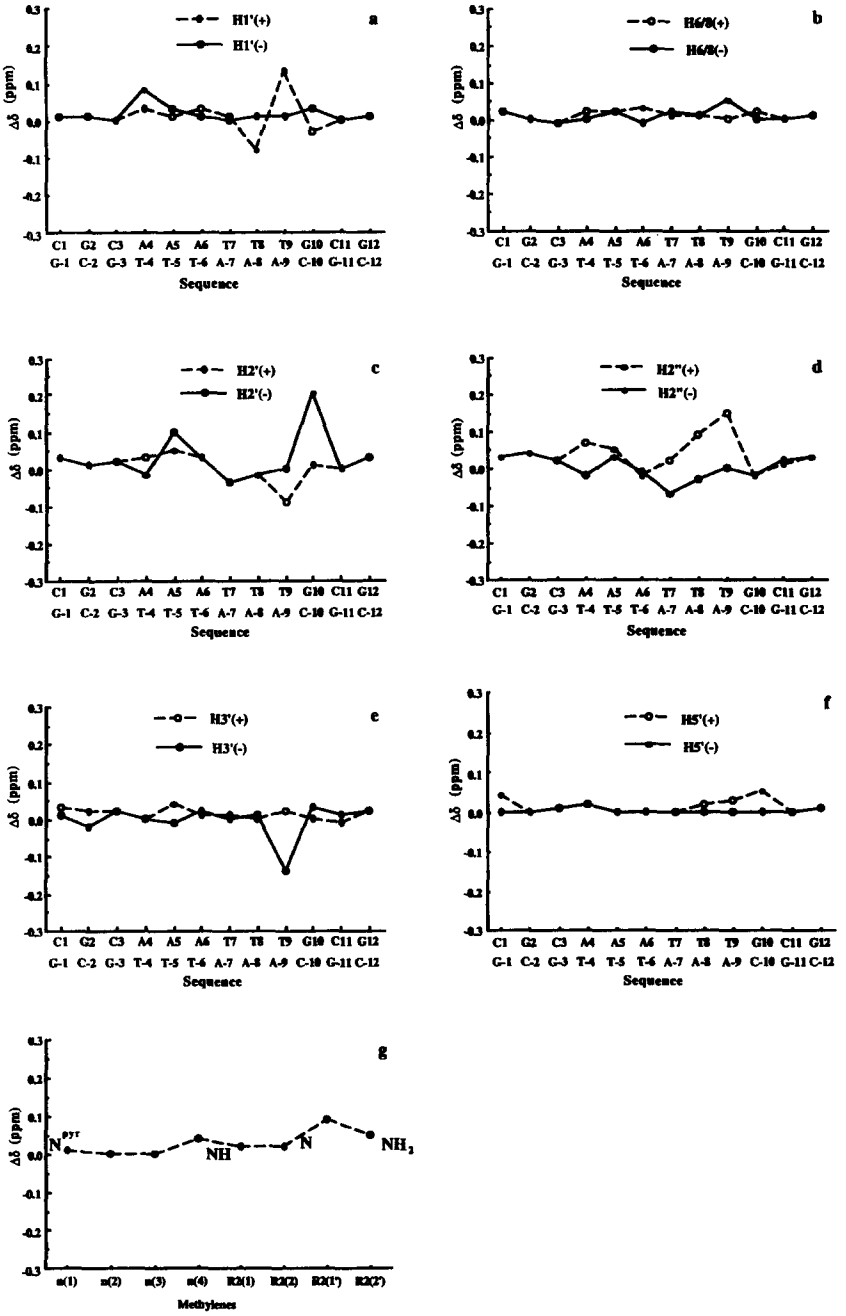

Figure 5. Induced chemical shift differences between the d(CGCA$_3$T$_3$GCG)$_2$:**6b**:Zn(II) complex and the d(CGCA$_3$T$_3$GCG)$_2$:**6b** complex vs the dsDNA sequence for the selected dsDNA protons: (a) H1'; (b) H6/8; (c) H2'; (d) H2"; (e) H3'; (f) H5'; (g) tren chain. $\Delta\delta = \delta_{Zn(II)\text{-complex}} - \delta_{Zn(II)\text{-free}}$. No significant changes were seen for the H5" protons.

constraints but the charge on the Zn(II) ion was reduced to +1 and zero. In these cases, the bending angle remained at *ca* 17.4° while the phosphate-to-phosphate distance on either side of the Zn(II) ion increased to 4.9 and 5.6 Å, respectively. The final two test minimizations included NOE constraints but the charge on the Zn(II) ion was reduced to +1 and zero. This led to bend angles of 33.8 and 34.5°, respectively, while the distance between the adjacent phosphates increased to 5.1 and 6.5 Å, respectively.

Electrophoretic mobility shift assay for 6b ± Zn(II) or La(III)

The effects of Zn(II)- and La(III)-bound **6b** on the electrophoretic mobility of ϕX-174-RF DNA *Hae*III restriction fragments were compared to **6b**'s effect on the same DNA fragments in the absence of metal ions. The migration of the DNA fragments showed inhibition with increasing concentrations of **6b** in the absence and presence of Zn(II) and La(III) (Fig. 7a). A plot of the

Table 4. Experimental (NOESY) and refined (restrained molecular modeling; in parentheses) distances for the $d(CGCA_3T_3GCG)_2$:**6b**:Zn(II) complex in D_2O[a]

(a) Distances involving only $d(CGCA_3T_3GCG)_2$ protons:

	H1'	H2'	H2"	H6/8	CH_3/H5
C_1 H6	3.1 (3.5)				
G_2 H8	4.3[b](4.4)	3.6[b](3.8)			
	3.9 (3.9)				
C_3 H5	4.4[b](4.4)		3.5[b](3.5)		
A_5 H8	3.9 (3.9)				
T_8 H6			3.6[b](3.7)		3.8[c](3.9)
T_8 CH_3				3.7[b](3.7)	
C_{11} H5			4.2[b](4.2)		
G_{12} H8	3.9 (3.9)	3.8[b](3.8)			
T_5 H6			4.2 (4.2)		3.7[c](3.7)

(b) Distances involving $d(CGCA_3T_3GCG)_2$ and **6b** protons:

H1–CH_3[R1]	3.7(4.2)	3.8[d](4.2)	H4–A_{-8}H2	3.1(3.1)	3.6[d](3.6)
H2–A_{-7}H2	3.0(3.0)	3.4[d](3.4)	H5–A_{-8}H2"	4.2(4.4)	
H2–T_{-5}H6	4.0(4.4)		H5–CH_2"(3)	3.6(4.2)	
H3–CH_2"(1)	3.0(2.9)	3.0[d](3.0)	H5–T_9H3'	5.5 (5.6)	
H4–A_{-8}H1'	4.4(4.6)	4.0[d](4.5)	H6–A_{-8}H2	3.5(3.7)	3.8[d](3.8)
H4–A_{-7}H2	3.7(3.7)	3.7[d](3.8)	H6–A_{-8}H1'	4.1(3.8)	4.0[d](4.2)
CH_2"(2)–T_9H3'	3.6(4.3)	3.8[d](4.2)	CH_3[R1]-A_6H1'	4.5(4.4)	4.2[d](4.2)
CH_2"(3)–T_9H3'	3.5(3.5)	3.6[d](3.6)			

[a]In Å, with the same residue.
[b]Distances with the (n-1) residue.
[c]Distances with the (n+1) residue.
[d]Distances for the $d(CGCA_3T_3GCG)_2$:**6b** complex.[15]

relative mobilities, R_L (the ratio of the apparent length to the real length, where the apparent length is determined from a standard curve of control DNA fragments), for the 1078 bp fragment vs [**6b**] is shown in Figure 7b. From this plot, it can be seen that addition of Zn(II) to **6b** decreases the effective size (increases mobility), relative to the control, of the DNA fragment to which it is bound. At the same time, La(III) bound to **6b** appears to slightly increase the effective size of the same DNA fragment.

A search for DNA cleavage by DNA-bound microgonotropen: metal ion complexes

The search for DNA cleavage was carried out using ^{32}P-labeled dsDNA fragments and supercoiled DNA. Dien-microgonotropen-a,b,c, dien, tren-microgonotropen-a,b and tren were incubated with 167 bp ^{32}P-labeled *Eco*RI/*Rsa*I pBR322 restriction fragments at 55 °C in the presence of metal ions as summarized in Table 5. No detectable specific hydrolytic cleavage was observed as evidenced by a lack of bands seen migrating below the full-length labeled DNA fragment on autoradiograms of the sequencing gels (data not shown). The presence of DNA bands corresponding to shorter than the full-length labeled DNA fragments (hence, cleavage products) indicated that some degradation occurred with the **6b** complexes of the Fe(II), Cu(II) and Ni(II) metal ions in the presence of H_2O_2 {for Fe(II)} or O_2 in conjunction with a reducing agent. These reactions were not reproducible (data not shown).

Supercoiled pBR322 DNA (175 μM) was incubated with up to 160 μM Co(II), Ni(II), Zn(II), La(III) or Ce(III) in the presence of up to 50 μM **6b** (pH 7.5 and 8.5) at 35 °C for as long as 24 h. To determine if these conditions produced any single- or double-stranded cleavage products, these reactions were analyzed by agarose gel electrophoresis. No nicking or other degradation was seen under these conditions (data not shown). However, 'complete' degradation (defined as all fragments migrating faster than and, hence, being shorter than the full-length DNA) of pBR322 was seen in the presence of 42 μM **6b** + 19 μM Cu(II) + 2.9 mM mercaptopropionic acid, pH 7.5, after ≥ 10 h incubating at 35 °C (data not shown). Incubation times of 5 min to 5 h led to both nicking and double-stranded cleavage, but not complete degradation.

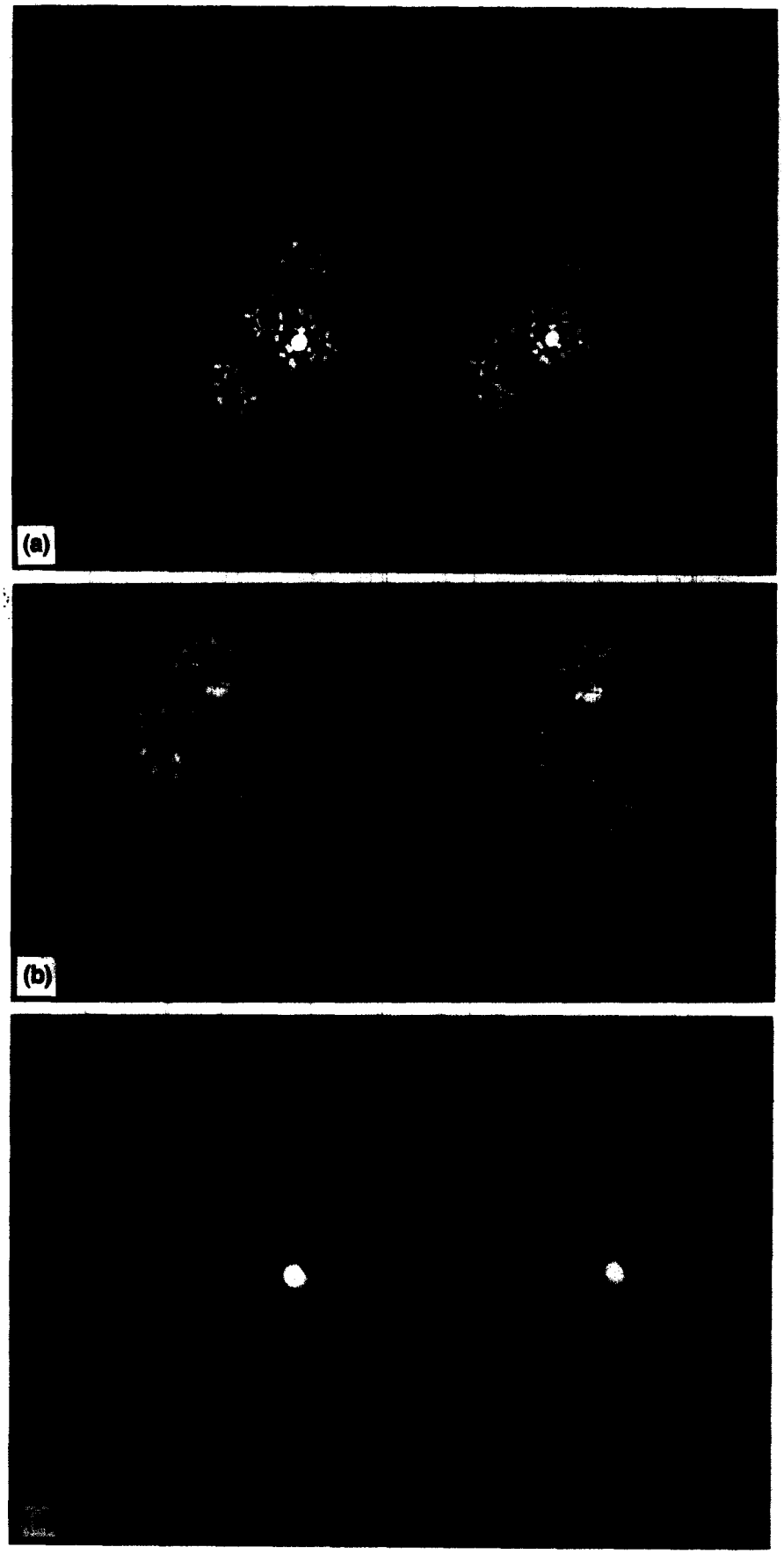

Figure 6. Stereo models of the D_2O solution structure of (a) the d(CGCA$_3$T$_3$GCG)$_2$:**6b**:Zn(II) complex, (b) a close-up view observing along the minor groove from the dimethylamino tail towards the acetamide terminus of **6b**, and (c) a close-up view of the two structures d(CGCA$_3$T$_3$GCG)$_2$:**6b**:Zn(II) {**6b** is magenta} and d(CGCA$_3$T$_3$GCG)$_2$:**6b** {**6b** is cyan} superimposed, based on a RMS fit to one another.

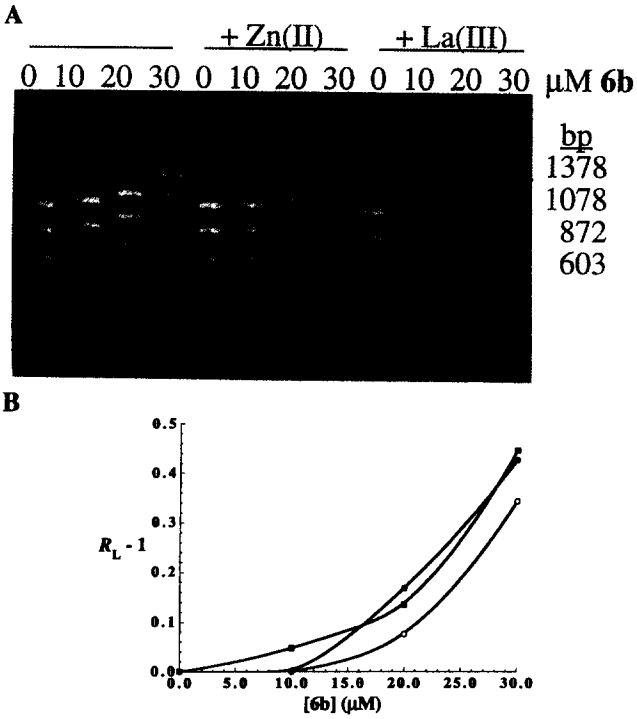

Figure 7. (a) Effect of DNA binding on the electrophoretic mobility of ϕX-174-RF DNA *Hae*III restriction digest fragments (sizes indicated at the right side of the figure). Lanes 1 – 4, control DNA at the indicated concentrations of **6b**; lanes 5 – 8, 300 μM Zn(II) at the indicated concentrations of **6b**; lanes 9 – 12, 300 μM La(III) at the indicated concentrations of **6b**. (b) A plot of the ratio of apparent DNA length to real length (relative to the control for each condition) minus 1 ($R_L - 1$) vs the concentration of **6b** in the absence (—l—) or the presence of $ZnCl_2$ (—m—) or $LaCl_3$ (—n—) for the 1078 bp DNA fragment. The curves are interpolations between the data points.

Discussion

Tren-microgonotropen-b (**6b**) has the very efficient metal binding tren {tris(2-aminoethyl)amine} substituent attached to its central pyrrole ring by a methylene linker arm. The association constant of tren for Zn(II) in water at 20 – 25 °C is greater than 3×10^{14} M^{-1}.[17,18] Ligation of Zn(II) by the tren moiety of **6b** neither enhances nor detracts from the equilibrium constant for binding of the latter to d(GGCGCA$_3$T$_3$GGCGG)/ d(CCGCCA$_3$T$_3$GCGCC) (Table 1). For these reasons, and since Zn(II) is diamagnetic and is a hydrolytically active metal ion, Zn(II) was chosen as an ideal metal ion for our studies.

The exchangeable and nonexchangeable proton resonances of d(CGCA$_3$T$_3$GCG)$_2$ provide supportive evidence for the formation of a 1:1 Zn(II)/ d(CGCA$_3$T$_3$GCG)$_2$:**6b** complex in the A+T-rich region of the dsDNA while ^{31}P NMR shows interaction of Zn(II) with the phosphate backbone. The solution structure of this complex was determined by two-dimensional ^{1}H NMR spectroscopy (NOESY) and restrained molecular modeling. Due to the complexity of ligation and the dynamics of **6b** in the complex with dsDNA and Zn(II), small populations of undetected free dodecamer or of dodecamer:ligand complexes other than those reported here may exist in solution.

Induced chemical shift differences (Δδ)

Induced chemical shift differences between the d(CGCA$_3$T$_3$GCG)$_2$:**6b**:Zn(II) and d(CGCA$_3$T$_3$GCG)$_2$:**6b** show that the polyamino substituent of **6b** {-(CH$_2$)$_4$N(CH$_2$CH$_2$)N(CH$_2$CH$_2$NH$_2$)$_2$} forms a four-coordinated Zn(II) complex that is in agreement with that found in the X-ray structure of 'tren-chloride':Zn(II). As expected, the chemical shift differences are small; however, they are consistent with the complexation of Zn(II) to the tren moiety. In the case of the sugar protons, the Δδ values are larger due to the distortion of the dsDNA molecule and/or to the repositioning of **6b** inside the minor groove. The values of Δδ reveal that the most affected protons involved in the dsDNA to **6b** interactions are H1' and H2'2" (Fig. 5). No effect was seen on the proton resonances of the aromatic bases indicating that the binding of Zn(II) does not significantly affect the positions of those protons that are major groove pointers. The Δδ for the H5' resonances shows that the position where the metal

Table 5. Conditions used in the search for DNA cleavage of the 167 bp ^{32}P-labeled *Eco*RI/*Rsa*I pBR322 restriction fragments with ligand:metal ion complexes at 55 °C (unless stated otherwise)[a]

Ligands	Metal ion	Reagents	pH	Time[b]
50 μM **6ab**, tren	Co(II), Ni(II), Zn(II), La(III), Ce(III)		5.6, 6.8, 8.0, 8.5	7 days
50 μM **5abc**	Co(II), Ni(II), Zn(II),La(III), Ce(III)		6.8	10 days
25 μM **5abc**	Co(II)	± 5 mM Im	6.8	60 min
50 μM **6ab**, tren	Co(III)		8.0	7 days
25 μM **5abc**	Ni(II), Zn(II)	± 5 mM Im	8.6	13 days
50 μM **5c**		La(III)	8.5	7 days
[c]50 μM **5abc**, **6ab**, dien, tren	Cu(II)	± 2 mM βME	7.8	180 min
50 μM **5abc**	Fe(II)	± 0.03% H_2O_2/ ± 4 mM DTT	7.0	60 min

[a]Each reaction mixture contained 1.0×10^{-9} mol (bp) of unlabeled calf thymus DNA; [metal ion] = 50 μM. Abbreviations: βME = β-mercaptoethanol; dien = 3,3'-iminobis(*N*,*N*-dimethylpropylamine); DTT = dithiothreitol; Im = imidazole; tren = tris(2-aminoethyl)amine.
[b]Time indicates maximum time incubated under given conditions.
[c]Incubated at 37 °C.

ion interacts with the phosphate backbone is P_9 and P_{10}. These observations are in agreement with the refined solution structure of the d(CGCA$_3$T$_3$GCG)$_2$:**6b**:Zn(II) complex (Fig. 6).

*The 3D solution structure of the d(CGCA$_3$T$_3$GCG)$_2$:**6b**:Zn(II) complex*

The position of the tripyrrole peptide of **6b** in the minor groove of the dsDNA changes very little upon complexing Zn(II) (Figs 2 and 4). The same five base pairs as in the d(CGCA$_3$T$_3$GCG)$_2$:**6b** complex (5'-$A_6T_7T_8T_9G_{10}$) are targeted. The terminal acetamide head is directed towards A_6 and the carboxy terminal dimethyl propylamino tail is towards G_{10}. Unlike observations with **6b** (as well as distamycin,[5] netropsin[19,20] or **5c**[11] and **6b**[15]), we did not see any exchange of **6b**:Zn(II) between two equivalent A_3T_3 sites. There was a decrease in the number of NOE interactions observed for H6/8 with CH_3/H5/6/8 protons (not involved in the exchange phenomena) as compared to the d(CGCA$_3$T$_3$GCG)$_2$:**6b** complex (Table 3). The loss of NOE interactions must be ascribed to the dynamic motion of the DNA molecule at the binding site while interacting with the Zn(II):**6b** complex (Table 3, see H6/8 interactions with CH_3/H5/6/8).

The protonated polyamine tren substituent of d(CGCA$_3$T$_3$GCG)$_2$:**6b** on ligation of Zn(II): (i) remains targeted for the P_9 and P_{10} phosphodiester linkages, (ii) brings about a 2 Å decrease in the P_9 to P_{10} distance, and (iii) increases the bending angle in the d(CGCA$_3$T$_3$GCG)$_2$:**6b**:Zn(II) complex by 14.6° as compared to d(CGCA$_3$T$_3$GCG)$_2$:**6b**. The tests of the NOE contraints (*vide supra*) and electrostatic charge of Zn(II) indicate that while much of the decrease in the distance between the phosphates was due to the attraction of the Zn(II) ion's positive charge or Zn(II)'s neutralization of the adjacent phosphates' negative charge, the bending in the solution structure was definitely directed by the NOE interactions. A comparison of d(CGCA$_3$T$_3$GCG)$_2$ solution structures with and without **5c**, **6b** and **6b**:Zn(II) is shown in Figure 8 emphasizing the differences in the bending angle. A molecular dynamics comparison of these solution structures in water is forthcoming.

Reduced electrophoretic mobilities on agarose gels of DNA restriction digest fragments after preincubation with **6b** have suggested a distortion of DNA conformation.[14] A change in DNA conformation was confirmed by direct visualization of DNA molecules complexed by **6b** with the aid of atomic force microscopy.[22] The current gel mobility shift assay indicates that there is little change in the electrophoretic mobility of DNA fragments when **6b**:Zn(II) is bound to DNA compared to **6b** alone. The distortion found might be related to the distortion of the tripyrrole peptide moiety as evidenced by the differences in the refined distances of the DNA:**6b** complexes with and without Zn(II). For example H4 is closer to A_{-8}H2 by 0.5 Å, while H6 becomes closer to A_{-8}H2 by 0.1 Å and H2 is closer to A_{-7}H2 by 0.4 Å (Table 4b). The T_9H3' sugar proton has closer proximities with the CH_2^n(3) protons of the hydrocarbon linker of **6b** by 0.1 Å but they are further from the CH_2^n(2) protons by 0.1 Å as compared to the complex without Zn(II). This is due to the tightening of the ligation at the metal ion site translated by the pulling of the polyamine substituent towards the phosphate backbone of the dsDNA and, consequently, the tilting of the tripyrrole peptide moiety inside the minor groove (Scheme 3). The tilt has a greater effect on the central pyrrole ring where the tren linker is attached, translated in smaller distances between H4 and A_{-8}H2 (0.5 Å, Table 4b) but a smaller effect on the flanking pyrroles (the distance decrease between H2 and A_{-7}H2 and between H6 and A_{-8}H2 is only 0.4 and 0.1 Å, respectively). The tightening of the ligation at the metal ion site affects the position of the terminal

Figure 8. A comparison of the space-filling models of solution structures of (a) d(CGCA$_3$T$_3$GCG)$_2$, (b) d(CGCA$_3$T$_3$GCG)$_2$:**5c**, (c) d(CGCA$_3$T$_3$GCG)$_2$:**6b**, and (d) d(CGCA$_3$T$_3$GCG)$_2$:**6b**:Zn(II). All structures are based on parameters and minimization procedures described in the Experimental section and are oriented to best visualize the bend (Figure S9) in the helical axis. This molecular graphics image was produced using the MidasPlus software from the Computer Graphics Laboratory, University of California, San Francisco.[21]

acetamide head as evidenced by distances that are 0.2 Å greater between the CH_3^{R1} and A_6H1' protons when compared to the complex without Zn(II) (Table 4b). The NOE determined distance (and minimized in parenthesis, Table 4) for the T_8H6 - T_7H2'' in the Zn(II) complex is shorter {3.6(3.7) Å} as compared to the dsDNA:**6b** complex {4.3(4.2) Å}. Shorter distances were also seen in the case of the T_8CH_3 – T_7H6 interaction {3.7(3.7) Å vs 4.3(4.4) Å}. We now see an additional NOE interaction between $T_{-5}H6$ and $T_{-5}H2''$ that was not seen in the case of the dsDNA:**6b** complex. Shorter distances were seen between the hydrocarbon linker of **6b** and the sugar protons at the binding site. The $CH_2''(2)$–T_9H3' distance is 3.6(4.3) vs 3.8(4.2) Å and the $CH_2''(3)$–T_9H3' distance is 3.5(3.5) vs 3.6(3.6) Å when comparing the complex with and without Zn(II). These indicate that the dsDNA bending is induced by the NOE distance constraints as a result of the tilting of the **6b** molecule inside the minor groove when complexed to Zn(II) (Scheme 3).

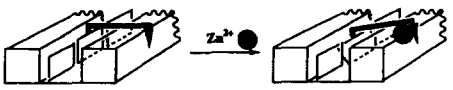

Scheme 3.

The coordination of Zn(II) to the four nitrogens of the tren substituent of **6b** leaves only a single open site on the Zn(II) of the **6b**:Zn(II) complex {occupied by Cl^- in the X-ray structure of 'tren chloride':Zn(II)[23]}. This positively charged open face interacts strongly with the negatively charged phosphate oxygens, embedding the Zn(II) ion in an electrostatic cage consisting of four nitrogens and an oxygen from each of two phosphates (Figs 6 and 9). With the metal ion embedded in this conformation, no catalytic site is available on Zn(II). This might explain the lack of hydrolytic cleavage found in the presence of the **6b**:Zn(II) complex and the small amount of cleavage seen with **6b** in the presence of other metal ions.

Conclusions

Microgonotropens can simultaneously ligate metal ions and bind dsDNA molecules. Evidence from ^1H NMR shows that the metallo-complexes of microgonotropens distort dsDNA molecules upon binding. The 1:1 complex of tren-microgonotropen-b (**6b**) with $d(CGCA_3T_3GCG)_2$ forms a ternary $d(CGCA_3T_3GCG)_2$:**6b**:Zn(II) metallo-complex and the solution structure of this complex has been characterized by 2D nuclear Overhauser effect ^1H NMR spectroscopy (NOESY) and restrained molecular modeling. The formation of the 1:1 Zn(II)/$d(CGCA_3T_3GCG)_2$:**6b** complex was monitored by ^1H NMR titration in the exchangeable and nonexchangeable proton regions. Results showed that the Zn(II) interacts with the A+T-rich region of the dsDNA. Comparison of the ^{31}P NMR spectra of the complexes with and without Zn(II) shows interaction with the phosphate backbone. Induced chemical shift differences between the $d(CGCA_3T_3GCG)_2$:**6b**:Zn(II) complex and $d(CGCA_3T_3GCG)_2$:**6b** show that the polyamino substituent of **6b** $\{-(CH_2)_4N(CH_2CH_2)N(CH_2CH_2NH_2)_2\}$ forms a four-coordinated Zn(II) complex that is in accord with that found in the X-ray structure of 'tren-chloride':Zn(II). The structure of the protonated polyamino substituent residing on the nitrogen of the central pyrrole ring changes upon Zn(II) complexation but does not change its initial target for the P_9 and P_{10} phosphodiester linkages. The dsDNA bending angle in the $d(CGCA_3T_3GCG)_2$:**6b**:Zn(II) complex increases 14.6° as compared to

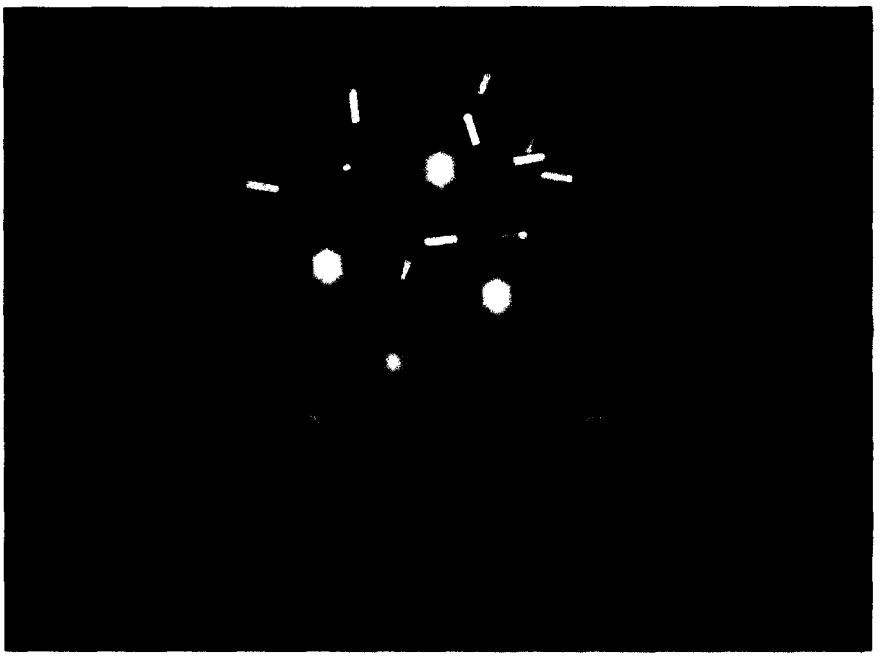

Figure 9. Mixed CPK and stick model of the $d(CGCA_3T_3GCG)_2$:**6b**:Zn(II) complex within a radius of 5 Å from Zn(II). The metal ion is embedded in an electrostatic cage consisting of four nitrogens and an oxygen from each of two phosphates.

d(CGCA$_3$T$_3$GCG)$_2$:**6b**. A decrease in the solvent accessible surface by 61 Å^2 upon binding of Zn(II) is in accord with the structure of **6b** becoming more compact when ligated to Zn(II). Unlike Barton's bis(tren:metal ion) DNA cleaving agent Ru(DIP)$_2$Macro^{n+} which efficiently cleaves plasmid DNA in the presence of metal ions,[24,25] the mono(ligand:metal ion) complexes formed with **5abc** and **6ab** do not cleave DNA to a detectable extent {except when the metal ion is Cu(II)}. When the metal ion is Cu(II) and incubation time is 5 h, **6b**:Cu(II) cuts plasmid DNA into a series of both singly- and multiply-cleaved plasmid molecules while Cu(II)$_2$(Ru(DIP)$_2$Macro)$^{6+}$ cleanly converts all of the supercoiled plasmid DNA into linearized full-length DNA in 1 h. Thus it appears that two ligands, each chelating a metal ion, are a necessary component in metal ion assisted cleavage of DNA.

Experimental

Reagents and methods for DNA binding studies

Reagents and methods for DNA binding studies were conducted as previously described with the sole addition of a constant concentration (1.0×10^{-7} M) of Zn(II) to each titration solution.[12,14]

The complex of d(CGCA$_3$T$_3$GCG)$_2$:6b

This has been reported.[15] Titration with Zn(II) was performed in 0.25 mol equivalents of $ZnCl_2$ (in 10 mM potassium phosphate buffer and 10 mM KCl at pH 7.0 in D_2O) at 21 °C to a solution of 2.5 mM d(CGCA$_3$T$_3$GCG)$_2$. The spectra were recorded 10 min after each addition.

The NMR sample for 2D ^{1}H NMR experiments

Samples contained 2.5 mM d(CGCA$_3$T$_3$GCG)$_2$:**6b** complex with 2.9 mM $ZnCl_2$ in 10 mM potassium phosphate buffer and 10 mM KCl at pH 7.0 with 0.1% 2,2-dimethyl-2-silapentane-5-sulfonate (DSS) in 0.4 mL D_2O (μ = 1.2). The solution was kept refrigerated at 4 °C between uses. All NMR spectra were recorded at 500 MHz on a GN-500 (General Electric) spectrometer at 10 °C, unless otherwise specified. Chemical shifts were referenced to the signal of DSS (0 ppm).

NOESY experiments

NOESY experiments were recorded in the phase sensitive mode using the hypercomplex NOE pulse sequence[26] with mixing times of 50, 100 and 180 ms for the d(CGCA$_3$T$_3$GCG)$_2$:**6b**:Zn(II) complex. Spectra were collected into 4 K complex points for 512 t_1 increments with a spectral width of 5681 Hz in both dimensions. The data matrix was zero filled to 2 K and appodized with a gaussian function to give a line broadening of 1 Hz in both frequency domains.

The ROESY experiment

The ROESY experiment was recorded at 10 °C using the Kessler pulse sequence[27] with a mixing time of 50 ms and a locking field strength of 2.5 kHz. The assignment of the ^{1}H chemical shifts generally followed the rules of assignment previously established.[28,29]

Distance calculations

Distance calculations were made as previously reported.[15]

Computational analysis and restrained molecular modeling

Computations were performed on a Silicon Graphics (Mountain View, CA) Iris 4D/340GTX workstation using CHARMm (version 21.3) and QUANTA (version 3.3.1) programs from Molecular Simulations, Inc. (Waltham, MA). Values for the sugar-phosphate backbone {O5'–PO$_4$–O3', O1P–PO$_4$–O2P, O3'–PO$_4$–O1P, O3'–PO$_4$–O2P, PO$_4$–O3'–C3', O3'–C3'–C4', C3'–C4'–C5', C4'–C5'–O5', C5'–O5'–PO$_4$, O5'–PO$_4$–O1P, O5'–PO$_4$–O2P} and the sugar-base {C2'–C1'–N1/N9, O4'–C1'–N1/N9} angles were from the AMBER force field (Version 3a).[30] The most notable changes in the parameters were 109.47° (CHARMm) to 119.9° (AMBER) and 109.47° (CHARMm) to 102.6° (AMBER) for the O1P–PO$_4$–O2P and O5'–PO$_4$–O3' angles, respectively. This is a reasonable change when one considers that the O1P–PO$_4$–O2P and O5'–PO$_4$–O3' angles for four published dsDNA crystal structures containing the sequence d(CGCA$_3$T$_3$GCG)$_2$ (2DND,[31] 1D63,[32] 1D65,[33] 121D[34]) have mean values of 115.9 ± 4.3° and 102.8 ± 4.2°, respectively. The solution structure of **6b** in a complex with d(CGCA$_3$T$_3$GCG)$_2$ was used as the initial coordinate for the minor groove binding and the methylene linker portions of the **6b**:Zn(II) complex.[15] In the 3D Molecular Editor routine of QUANTA, a tren moiety complexed to Zn(II) {Cambridge Structural Databank (version 5.06, October 1993 release; Cambridge, U.K.)[35] refcode = AEZNPB[23]} was used to replace the tren moiety of the previously determined structure of **6b** when it is complexed to d(CGCA$_3$T$_3$GCG)$_2$. This **6b**:Zn(II) structure was docked into the solution structure for free d(CGCA$_3$T$_3$GCG)$_2$.[15] The tren-microgonotropen was then oriented such that the through space proton interactions seen in the NOESY experiment were brought into close proximity with each other. This was the structure used to initiate the structural refinement of the 1:1 complex of d(CGCA$_3$T$_3$GCG)$_2$:**6b**:Zn(II). As with the d(CGCA$_3$T$_3$GCG)$_2$:**6b** structure,[15] only two Na^+ gegenions (instead of four for the **5c** structure)[11] were removed from the vicinity of the phosphates nearest to where the tren/Zn(II) moiety was initially located. Atomic partial charges of the atoms in **6b** and d(CGCA$_3$T$_3$GCG)$_2$ were generated from CHARMm's force field's parameter files. The zinc ion had a fixed charge of +2 while the tertiary dimethylamino tail of **6b** was modeled protonated (partial charge of +0.35) leading to a total charge of +3 for **6b**.

CHARMm minimization procedures were as previously described for d(CGCA$_3$T$_3$GCG)$_2$:**6b**[15]: *in vacuo*; distance constraint forces ranged up to 500 kcal mol^{-1} Å^{-2} depending upon the upper and lower limits for a given NOE derived value; a radially dependent distance dielectric with $\varepsilon = R$ was used to account for solvent effects; the nonbonded cut-off distance was 15 Å while the nonbonded and energy lists were updated every five steps; 100 steps of steepest descents minimization were followed by the adopted basis Newton–Raphson (ABNR) algorithm until the root mean square derivative reached < 0.5 kcal mol^{-1}·Å^{-1}. Backbone dihedral angle and base pairing distance constraints for the DNA were not included in the simulations.

Parameters and constraints for the tren:Zn(II) complex had to be derived since the CHARMm program does not provide these parameters and, hence, cannot interpret ligand to metal ion interactions such as those being modeled. When parameters were not available from CHARMm, the bond distances, angles and dihedral angles were based on average values from the Cambridge Structural Databank crystal structures AEZNPB[23] and VICXEK.[36] Forces for which parameters were estimated were adjusted until refined parameters were within 1, 3, or 1 standard deviation(s) of the respective mean bond distances, bond angles and dihedral angles found in the crystal structures (Tables 6 – 8). A new CHARMm atom type, NTZ, was created to account for a tetrahedral tertiary amine ligating to a zinc ion. Thus, Zn(II) was held essentially fixed by the tren moiety as in the crystal structures AEZNPB (Chart 1) and VICXEK.

The same four crystal structures used to measure the sugar-phosphate backbone angles were used to determine the mean adjacent phosphate-to-phosphate distances (e.g. P_9 to P_{10}; sample size was 80 distances). The molecular contact surface area was determined using Connolly solvent accessible surface calculations[37] in QUANTA with a radius of 1.4 Å to simulate a water molecule sized probe (Na^+ counterions were not included in the calculations). The result of the calculation for the DNA:**6b**:Zn(II) complex was subtracted from the result for the same DNA with **6b**:Zn(II) removed from the binding site. This yielded the surface of the DNA that was inaccessible to the probe due to the presence of **6b**:Zn(II). The method for the measurement of the extent of solution structural changes was described previously[15] using Dickerson's NEWHEL93 program.[38]

Electrophoretic mobility assay

The final concentrations (10 µL) of all reactions were 150 µM (in bp) of ϕX-174-RF DNA *Hae*III restriction digest (Pharmacia) in 10 mM Tris–HCl, pH 7.5, 50 mM KCl. Incubation of DNA with **6b** (0, 10, 20 or 30 µM) ± 300 µM $ZnCl_2$ or $LaCl_3$ was for 60 min at room temperature. At this time, 2 µL of loading buffer 40% (w/v) sucrose, 0.25% bromophenol blue, and 0.25% xylene cyanol[39] was added to each sample. Samples

Table 6. Bond distance parameters used for modeling Zn(II) complexed to the tren moiety of **6b**[a]

Atom 1	Atom 2	Distance (Å)	Force constant (kcal mol^{-1} Å^{-2})
CT[b]	NTZ	1.453	275
MZN[c]	NT	2.073 ± 0.023	375
MZN[c]	NTZ	2.191 ± 0.190	375

[a]CT = tetrahedral carbon, NTZ = tetrahedral nitrogen bound to Zn(II), MZN = zinc atom, and NT = tetrahedral nitrogen.
[b]Based on CHARMm's values for CT to NT.
[c]Based on mean values of the bond distances found in the crystal structures AEZNPB and VICXEK, plus or minus the standard deviation, σ_n.

Table 7. Bond angle parameters used for modeling Zn(II) complexed to the tren moiety of **6b**[a]

Atom 1	Atom 2	Atom 3	Angle (°)	Force constant (kcal mol^{-1} rad^{-2})
CT[b]	CT	NTZ	110.5	85
CT[c]	NTZ	CT	110.5	52
HA[d]	CT	NTZ	109.5	60
HC[e]	NT	MZN	107.0	35
CT[f]	NT	MZN	110.2 ± 1.02	85
CT[f]	NTZ	MZN	106.9 ± 1.07	85
NT[f]	MZN	NT	117.5 ± 3.21	80
NTZ[f]	MZN	NT	81.2 ± 2.30	70

[a]HA = aliphatic or aromatic hydrogen, and HC = charged hydrogen. See footnote (a) from Table 6 for other atom abbreviations.
[b]Based on CHARMm's values for CT to CT to NT.
[c]Based on CHARMm's values for CT to NT to CT.
[d]Based on CHARMm's values for CT to CT to NT.
[e]Based on CHARMm's values for MCU (copper atom) to NT to HC.
[f]Based on mean values of the bond angles found in the crystal structures AEZNPB and VICXEK, plus or minus the standard deviation, σ_n.

Table 8. Dihedral angle constraints used for modeling Zn(II) complexed to the tren moiety of **6b**[a]

Atom 1	Atom 2	Atom 3	Atom 4	Angle (°)	Force constant (kcal mol^{-1} rad^{-2})
CT[b]	NTZ	CT	CT	0.0	0.40
CT[c]	NTZ	CT	HA	180.0	0.10
HA[c]	CT	NTZ	MZN	180.0	0.10
CT[d]	CT	NTZ	MZN	−31.7 ± 1.87	50.0
CT[d]	CT	T	MZN	−40.4 ± 10.4	50.0
CT[d]	NT	MZN	NTZ	17.2 ± 7.62	50.0
CT[d]	NT	MZN	NT	92.3 ± 4.75	50.0
				−57.8 ± 11.3	50.0
CT[d]	NTZ	MZN	NT	127.7 ± 5.13	50.0
				7.72 ± 4.61	50.0
				−111.6 ± 4.05	50.0

[a]See footnote (a) from Tables 6 and 7 for atom abbreviations.
[b]Based on CHARMm's values for CT to CT to NT to CT.
[c]Based on CHARMm's values for HA to CT to NT to H.
[d]Based on mean values of the dihedral angles found in the crystal structures AEZNPB and VICXEK, plus or minus the standard deviation, σ_n. These dihedral angles were maintained by the use of dihedral constraints.

were electrophoresed through a 4% NuSieve 3:1 (FMC BioProducts) agarose gel in 40 mM Tris–acetate, pH 7.8 for 6 h at 2 V cm^{-1}. The gel was stained with a 0.5 μg mL^{-1} solution of ethidium bromide in deionized water for 30 min, destained for 30 min in deionized water, and photographed on a UV (302 nm) transilluminator with Polaroid type 667 film.

DNA cleavage studies

Performed as follows: The 167 bp ^{32}P-labeled *Eco*RI/*Rsa*I DNA fragment and the dideoxy DNA sequencing ladders of pBR322 were generated as previously described for DNA footprinting.[1,14] Dien-microgonotropen-a,b,c {**5a,b,c**}, tren-microgonotropen-a,b {**6a,b**}, 3,3'-iminobis(*N,N*-dimethylpropylamine) {dien}, and tris(2-aminoethyl)amine {tren} at 20 – 50 μM were mixed with the ^{32}P-labeled pBR322 fragment ($1 - 10 \times 10^4$ cpm μL^{-1}) and 40 – 100 μM calf thymus DNA in 20 – 50 μL total volumes. These samples were incubated under a layer of Nujol oil at 55 °C {except for Cu(II) which was at 37 °C} ± metal ions under the condition shown in Table 5. Solutions contained 50 mM KCl and were buffered with MES·KOH or Tris–HCl. Reactions were stopped by removing the solutions from under the oil and precipitating the DNA with ammonium acetate, ethanol and 600 μg mL^{-1} tRNA (brewer's yeast; Boehringer Mannheim). After drying, the samples were resuspended in 4 μL formamide loading buffer, heated to 90 °C for 5 min, and loaded on a prewarmed 8% (w/v) hydrolink monomer (AT Biochem's LongRanger) gel (30 × 40 cm × 0.04 cm) which contained 50% (w/v) urea (89 mM Tris–borate, 2 mM EDTA). The reaction products were coelectrophoresed with the sequencing products at *ca* 50 °C (75 W, constant power) for 90 min. After electrophoresis, gels were dried at 80 °C under vacuum. Autoradiography was for 1 – 7 days with an intensifying screen.

Cleavage of 175 μM supercoiled pBR322 DNA (Pharmacia) by metal ions {160 μM Co(II), 160 μM Ni(II), 35 – 350 μM Zn(II), 160 μM La(III), 1.4 – 160 μM Ce(III), or 1.4 – 160 μM Cu(II) + 5.8 mM mercaptopropionic acid} in the presence of 7 – 50 μM **6b** was assessed at 35 °C. The 20 μL reactions were run for 1 – 24 h in 10 mM Tris–HCl, pH 7.5 or 8.5, 50 mM KCl. At completion, 2.2 μL of loading buffer {10% (w/v) glycerol, 0.1% (w/v) sodium dodecyl sulfate, and 0.1% (w/v) bromophenol blue}[39] was added to each sample. The products were separated by electrophoresis on a 100 mL 1% ultrapure agarose (Bethesda Research Laboratories) gel in 40 mM Tris–acetate, pH 8.0 and 1 mM EDTA for 3 h at 3.3 V cm^{-1}. The gel was stained and photographed as for the electrophoretic mobility shift assays.

Acknowledgements

This work was supported by grants from the Office of Naval Research and the National Science Foundation. We wish to thank Professor John Carbon for use of his laboratory space for ^{32}P-labeled DNA experiments and Dr Jay C. Groppe for his assistance in the ^{32}P-labeled DNA experiments.

References

1. Sigel, H. In: *Metal–DNA Chemistry*, Vol. 402, pp. 159–199, Tullius, T. D., Ed.; ACS Symposium Series, ACS; Washington D.C., 1989.
2. Jenkins, T. C.; Lane, A. N.; Neidle, S.; Brown, D. G. *Eur. J. Biochem.* **1993**, *213*, 1175.
3. Blaskó, A.; Bruice; T. C. *Proc. Natl Acad. Sci. U.S.A.* **1993**, *90*, 10018.
4. Chen, X.; Ramakrishnan, B.; Rao, S. T.; Sundaralingam, M. *Struct. Biol.* **1994**, *1*, 169.
5. Pelton, J. G.; Wemmer, D. E. *J. Am. Chem. Soc.* **1990**, *112*, 1393.
6. Geierstanger, B. H.; Dwyer, T. J.; Bathini, Y.; Lown, J. W.; Wemmer, D. E. *J. Am. Chem. Soc.* **1993**, *115*, 4474.
7. Gao, X.; Mirau, P.; Patel, D. J. *J. Mol. Biol.* **1992**, *223*, 259.
8. Haworth, I. S.; Elcock, A. H.; Rodger, A.; Richards, W. G. *J. Biomol. Struct. Dyn.* **1991**, *9*, 553.
9. Harding, M. M.; Harden, G. H.; Field, L. D. *FEBS Lett.* **1993**, *322*, 291.

10. He, G.-X.; Browne, K. A.; Groppe, J. C.; Blaskó, A.; Mei, H.-Y.; Bruice, T. C. *J. Am. Chem. Soc.* **1993**, *115*, 7061.

11. Blaskó, A.; Browne, K. A.; He, G.-X.; Bruice, T. C. *J. Am. Chem. Soc.* **1993**, *115*, 7080.

12. Browne, K. A.; He, G.-X.; Bruice, T. C. *J. Am. Chem. Soc.* **1993**, *115*, 7072.

13. Bruice, T. C.; Mei, H.-Y.; He, G.-X.; Lopez, V. *Proc. Natl Acad. Sci. U.S.A.* **1992**, *89*, 1700.

14. He, G.-X.; Browne, K. A.; Blaskó, A.; Bruice, T. C. *J. Am. Chem. Soc.* **1994**, *116*, 3716.

15. Blaskó, A.; Browne, K. A.; Bruice, T. C. *J. Am. Chem. Soc.* **1994**, *116*, 3726.

16. Saenger, W. *Principles of Nucleic Acid Structure*, Springer; New York, 1984.

17. Ackermann, von H.; Schwarzenbach, G. *Helv. Chim. Acta* **1949**, *32*, 1543.

18. Rabenstein, D. L.; Blakney, G. *Inorg. Chem.* **1973**, *12*, 128.

19. Patel, D. J.; Shapiro, L. *Biochimie* **1985**, *67*, 887.

20. Patel, D. J. ; Shapiro, L. *J. Biol. Chem.* **1986**, *261*, 1230.

21. Ferrin, T. E.; Huang, C. C.; Jarvis, L. E.; Langridge, R. *J. Mol. Graphics* **1988**, *6*, 13.

22. Hansma, H. G.; Browne, K. A.; Bezanilla, M.; Bruice, T. C. *Biochemistry* **1994**, *33*, 8436.

23. Sime, R. J.; Dodge, R. P.; Zalkin, A.; Templeton, D. H. *Inorg. Chem.* **1971**, *10*, 537.

24. Basile, L. A.; Barton, J. K. *J. Am. Chem. Soc.* **1987**, *109*, 7548.

25. Basile, L. A.; Raphael, A. L.; Barton, J. K. *J. Am. Chem. Soc.* **1987**, *109*, 7550.

26. States, D. J.; Haberkorn, R. A.; Ruben, D. J. *J. Magn. Reson.* **1982**, *48*, 286.

27. Kessler, H.; Griesinger, C.; Kerssebaum, R.; Wagner, E.; Ernst, R. *J. Am. Chem. Soc.* **1987**, *109*, 607.

28. Hare, D. R.; Wemmer, D. E.; Chou, S.-H.; Drobny, G.; Reid, B. R. *J. Mol. Biol.* **1983**, *171*, 319.

29. Patel, D. J.; Shapiro, L.; Hare, D. *Q. Rev. Biophys.* **1987**, *20*, 35.

30. Weiner, S. J.; Kollman, P. A.; Nguyen, D. T.; Case, D. A. *J. Comp. Chem.* **1986**, *7*, 230.

31. Coll, M.; Frederick, C. A.; Wang, A. H.-J.; Rich, A. *Proc. Natl Acad. Sci. U.S.A.* **1987**, *84*, 8385.

32. Brown, D. G.; Sanderson, M. R.; Garman, E.; Neidle, S. *J. Mol. Biol.* **1992**, *226*, 481.

33. Edwards, K. J.; Brown, D. G.; Spink, N.; Skelly, J. V.; Neidle, S. *J. Mol. Biol.* **1992**, *226*, 1161.

34. Tabernero, L.; Verdaguer, N.; Coll, M.; Fita, I.; van der Marel, G. A.; van Boom, J. H.; Rich, A.; Aymamí, I. *Biochemistry* **1993**, *32*, 8403.

35. Allen, F. H.; Kennard, O.; Taylor, R. *Acc. Chem. Res.* **1983**, *16*, 146.

36. Lu, Q.; Luo, Q. H.; Dai, A. B.; Zhou, Z. Y.; Hu, G. Z. *J. Chem. Soc., Chem. Comm.* **1990**, 1429.

37. Connolly, M. L. *Science* **1983**, *221*, 709.

38. Prive, G. G.; Yanagi, K.; Dickerson, R. E. *J. Mol. Biol.* **1991**, *217*, 177. NEWHEL93 was generously provided by R. E. Dickerson. The program was run on a Silicon Graphics Iris 4D/340GTX workstation with coordinates in Brookhaven's Protein Data Bank format. The best helices were generated from the sugars' C1', the pyrimidine's N1, and the purine's N9 atoms.

39. Sambrook, J.; Fritsch, E. F.; Maniatis, T. *Molecular Cloning, A Laboratory Manual*, 2nd Edition, Cold Spring Harbor, New York, 1989.

Supplementary material available from the authors

Table S1: ^{1}H Chemical shifts for **6b** in the d(CGCA$_3$T$_3$GCG)$_2$:**6b** complex and in the d(CGCA$_3$T$_3$G CG)$_2$:**6b**:Zn(II) complex in D_2O. **Figure S1**: ^{1}H NMR titration spectra in the 1.0 – 3.5 ppm region of 2.5×10^{-3} M d(CGCA$_3$T$_3$GCG)$_2$:**6b** in 9:1 H_2O:D_2O (10 mM phosphate buffer, pH 7.0, 10 mM KCl) with $ZnCl_2$ at 21 °C at the indicated mole ratios of Zn(II)/d(CGCA$_3$T$_3$GCG)$_2$:**6b**. **Figure S2:** ^{31}P NMR spectra of d(CGCA$_3$T$_3$GCG)$_2$:**6b**:Zn(II) and d(CGCA$_3$T$_3$GCG)$_2$:**6b** at 2.5×10^{-3} M in D_2O and 21 °C. **Figure S3:** Expansion of the NOESY spectrum of d(CGCA$_3$T$_3$GCG)$_2$:**6b**:Zn(II) in the (5.3 – 8.5) × (5.2 – 8.5) ppm region. **Figure S4:** *ibid*, in the (1.4 – 3.1) × (4.4 – 6.3) ppm region. **Figure S5**: *ibid*, in the (1.0 – 3.5) × (1.0 – 3.5) ppm region. **Figure S6**: *ibid*, in the (3.3 – 6.9) × (3.3 – 6.9) ppm region. **Figure S7**: *ibid*, in the (3.6 – 5.2) × (7.0 – 8.4) ppm region. **Figure S8**: ROESY spectrum of d(CGCA$_3$T$_3$GCG)$_2$:**6b**:Zn(II). **Figure S9:** Normal vector plots to the mean plane of the base pairs for the d(CGCA$_3$T$_3$GCG)$_2$, d(CGCA$_3$T$_3$GCG)$_2$:**5c**, d(CGCA$_3$T$_3$GCG)$_2$:**6b**, and d(CGCA$_3$T$_3$GCG)$_2$:**6b**: Zn(II) complexes (10 pages available upon request from the authors).

(*Received in U.S.A. 27 September* 1994; *accepted* 3 *January* 1995)